# Liquid Crystalline Properties and Molecular Packing of Semifluorinated *n*-Alkanes $F(CF_2)_{10}(CH_2)_mH$

**Masakazu Fujiwara,*,† Katsuhiko Satoh,‡ Shoichi Kondo,§ and Seiji Ujiie||**

*KYOCERA CHEMICAL Corporation, 5-14-25, Ryoke, Kawaguchi, Saitama 332-8533, Japan; College of General Education, Osaka Sangyo University, 3-1-1, Nakagaito, Daito-shi, Osaka 574-8530, Japan; Department of Chemistry, Tokyo University of Science, 1-3 Kagurazaka, Shinjuku, Tokyo 162-8601, Japan; and Department of Applied Chemistry, Faculty of Engineering, Oita University, Oita 870-1192, Japan*

*Received November 11, 2005; Revised Manuscript Received June 11, 2006*

ABSTRACT: The phase transitions for a homologous series of semifluorinated *n*-alkanes, $F(CF_2)_{10}(CH_2)_mH$, with $2 \leq m \leq 19$ (F10H*m*), have been characterized using a polarizing microscope, DSC, X-ray diffraction, and dilatometry. Thermal analysis and optical textures indicate the presence of the smectic−smectic phase transition when the number of methylene units ranges from 6 to 12. The phase-transition temperature depends on the length (*m*) of the hydrocarbon segment. The density decreases with increases in the carbon number of the hydrogen segment. The data for both the thermal properties and the density suggest that the smectic−smectic phase transition is significantly first-order, which is primarily caused by a change in the molecular packing for the molecular rearrangement, while a transition for the clearing point is related to disordering of the entire molecule. The volume jump shows that F10H*m* have the same molecular packing in the high-temperature mesophase and that their magnitude is greater than that of the conventional liquid crystalline compounds having an aromatic−mesogenic core. The effects of the fluorinated segment for the phase transitions are also discussed herein.

## Introduction

Fluorocarbons and hydrocarbons are poorly miscible because the conformation and electrostatic interactions of the fluorocarbons are different from those of hydrocarbons. In general, fluorocarbons adopt a 15/7 helical structure by an intermolecular steric repulsion of the fluorine atoms along the carbon backbone, whereas hydrocarbons favor the well-known planar zigzag conformation. Semifluorinated *n*-alkanes $F(CF_2)_n(CH_2)_mH$ (F*n*H*m*) consequently undergo mesophase−mesophase, mesophase−solid, and/or solid−solid transitions.[1−10] These diblock molecules are of considerable interest because they have a different and unique structure from a normal mesogen containing a rigid core and flexible chains.

As a result of two incompatible segments, the semifluorocarbons can form Langmuir films at the air−water interface as well as amphiphiles with a hydrophilic headgroup.[9,11−13] Moreover, highly stable molecular layers prepared by a self-assembling method have been applied for the development of various detection systems such as electrochemical detection, optical detection, and so on. The self-assembled monolayers (SAMs), which are crystalline chemisorbed organic single layers, are formed on a solid substrate by the spontaneous organization of molecules. Semifluorinated alkanethiols generate SAMs by the adsorption of $F(CF_2)_n(CH_2)_mSH$ onto gold, and they produce extremely low surface energy and highly hydrophobic surface coatings; they are regarded as one of the most studied compounds.[14] Moreover, semifluorinated *n*-alkanes are now being watched with keen interest, functioning as an internal tamponade agent that has greatly facilitated vitreoretinal surgery against retinal detachment.[15] The effectiveness of these substances as internal tamponade agents is reported to be due to their ability to fill model eye chambers and the vitreous cavity.

Comprehensive studies of transition behavior have been presented for F12H*m*, with *m* being an even number of carbon atoms ranging from 2 to 20 by DSC, Raman spectroscopy, SAXS, and WAXD.[1,2] The structures for an isolated chain and possible packing in the crystal lattice have also been studied by semiempirical and molecular field methods. F12H*m* with $m \leq 6$ has only one sharp peak in the SAXS profile, with layer spacing that is less than the molecular length. The compounds therefore form monolayers in which the molecular axes are tilted with respect to the layer normal below the solid−solid transition. For $8 \leq m \leq 14$, the profile consists of four peaks due to the coexistence of a high-temperature phase with a low-temperature phase. The crystal is then formed by an interleaved bilayer structure. When $14 \leq m$, only a single sharp reflection appears, which is less than twice the molecular length. On the other hand, a series of F10H*m* have been studied regarding the layer structure for F10H10.[1,4,5] This compound has been found to present a liquid crystal−liquid crystal transition above room temperature. The transformation between the structures is achieved by a change in the tilt angles. The dielectric behavior for F*n*H*m* has also been investigated.[16,17] Especially, for F10H10 and F12H8, which have very similar lengths, the apparent difference in the activation energy and dipole moment between the two compounds leads to a difference in the rotational motion of the fluorocarbon segments.[16]

Despite the many experiments that have been carried out, the densities of the semifluorinated *n*-alkanes are not yet known due to measurement difficulties. Knowing the precise density for the systems would make it possible to have a detailed discussion on molecular packing in the mesophase. In this study, the phase transition and packing information for the molecules with hydrocarbons and fluorocarbons of 10 carbon atoms were investigated using dilatometry together with a polarizing

* To whom correspondence should be addressed. E-mail: masakazu.fujiwara@kyocera-chemi.jp.
† KYOCERA CHEMICAL Corporation.
‡ Osaka Sangyo University.
§ Tokyo University of Science.
|| Oita University.

10.1021/ma052411b CCC: $33.50 © 2006 American Chemical Society
Published on Web 07/22/2006

**Table 1. Transition Temperatures and the Corresponding Entropies by DSC for F10H*m***

| *m* | $T_{M2-M1}$/K | $\Delta S_{M2-M1}$/ J K$^{-1}$ mol$^{-1}$ | $T_{M1-iso}$/K | $\Delta S_{M1-iso}$/ J K$^{-1}$ mol$^{-1}$ |
|---|---|---|---|---|
| 2 | | | 292.8 | 19 |
| 5 | | | 307.5 | 59 |
| 6 | 303.5 | 15 | 314.5 | 54 |
| 7 | 302.8 | 19 | 321.3 | 61 |
| 8 | 298.0 | 21 | 326.0 | 68 |
| 9 | 305.9 | 24 | 330.0 | 75 |
| 10 | 305.5 | 6 | 332.8 | 85 |
| 11 | 323.5 | 30 | 334.4 | 97 |
| 12 | 332.6 | 33 | 335.3 | 103 |
| 13 | | | 337.8 | 125 |
| 14 | | | 340.4 | 137 |
| 15 | | | 342.1 | 145 |
| 16 | | | 344.5 | 157 |
| 17 | | | 346.0 | 171 |
| 18 | | | 348.1 | 176 |
| 19 | | | 349.2 | 186 |

microscope, differential scanning calorimetry (DSC), and an X-ray diffraction study.

## Experimental Section

The semifluorinated *n*-alkanes F10H*m* with $m = 2$, 5, and 6−19 were synthesized using the methods of Höpken et al.[6] and Rabolt et al.[1] These materials were purified by several recrystallizations from methanol/acetone and by Kugelrohr distillations to produce products as white powders. The final products were characterized by gas chromatography, $^1$H NMR spectroscopy, mass spectroscopy, and elemental analysis. Purities were better than 99%. Optical micrographs were recorded using an OLYMPUS BH-2 polarizing microscope equipped with a Mettler FP82 hot stage and an FP80 central processor. Thin layers of the compounds were obtained by melting a small amount of the solid powders placed on a microscopic slide and covered with a coverslip. DSC measurements were performed with a Mettler TA3000. The temperatures and heats of transition were calibrated using indium as a standard material. Specimens of 1 mg and a constant heating/cooling rate of 1 K/min were used to conduct the experiments at conditions close to thermal equilibrium. X-ray diffraction measurements were performed using a Rigaku RINT2100 diffractometer with a heating stage and Ni-filtered Cu Kα radiation. The density was measured with the use of a capillary type dilatometer, according to the method described by Guillon and Skoulios.[18] The dilatometer's capillary tube was ∼0.5 mm, which was calibrated using distilled mercury. The dilatometer, filled with ∼0.5 g of the sample, was immersed in a large oil bath, the temperature of which was regulated to within 0.05 K. The scanning rate was ∼2 K/h. The variation in density was determined from reading the height of the mercury column, and the density measurements were accurate to ±0.0001 g cm$^{-3}$. The mercury level was read with a cathetometer. The optimized geometries of F10H*m* were estimated by ab initio calculations with B3LYP/6-311G** using the Gaussian 03 package.[19]

## Results and Discussion

**Transition Temperature and Texture.** Table 1 shows the DSC data for the studied compounds. The F10H*m* specimens with $6 \le m \le 12$ show the melting endotherm and other endothermeric transitions below the clearing point. Figure 1 shows the variation in the transition temperature determined by DSC measurement with respect to the length of the hydrocarbon segment of all the compounds studied. The values for $m = 8-12$ were in fairly close agreement with those by Rabolt et al.[1] and Viney et al.[4,5] The phase behavior of the compounds depends on the thermal hysteresis of the sample, except for $m = 6$. The clearing temperatures increase with the increases in the carbon number of the hydrogen segment. The compounds ranging in hydrogenated carbon atoms from 6 to 12 were found to exhibit

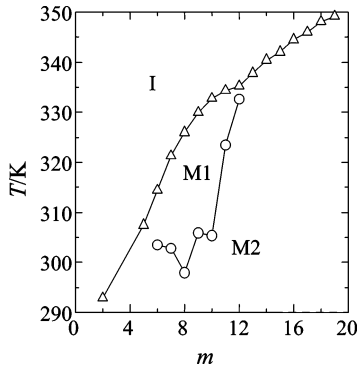


**Figure 1.** Phase transition temperature (open circles) and clearing point (open triangles) of F10H*m* as a function of the length *m* of the hydrocarbon segment.

a mesophase−mesophase transition below the clearing temperature. These compounds show an irregularity in the transition temperatures from a lower temperature phase (M2) to a higher one (M1). This result suggests a different structure in the M2 phase or a diversity of molecular packing with the protonated segment.

Figure 2 shows the polarizing microscopic texture at various temperatures for F10H10. The optical texture in the M1 phase is shown in Figure 2a. The lancet-like morphology and the homeotropic black are more likely to have the characteristic texture of a smectic B phase rather than the other smectic phases. The layer planes of the molecules are parallel to the glass surface, and the texture is viewed through a microscope perpendicular to the layer plane, with a black field of view. The black areas turned bright when the sample was tilted or sheared. Figure 2b shows a texture in the M2 phase in which the main domain remains unchanged, and striations or flaws appear in the domain. For $m = 6$ and 7, the striations in the M2 phase are perpendicular to the length of the original M1 domain; in contrast, with $m = 8$ the striations are parallel. On the other hand, when $9 \le m \le 12$, a great number of flaws appeared in addition to the random striations in the M2 phase. It is important to note that this texture in the M2 phase of F10H10 seems to be metastable, as it dramatically becomes mosaic-like after ∼1 day, as shown in Figure 2c. This result was fairly similar to that obtained with F10H5, as shown in the next picture. A relatively long time was required to obtained equilibrium with F10H10. This phenomenon was never occurred for the other compounds and is likely related to the extremely slow kinetics in the transition from the M1 to the M2 phase. The M2 phase can be regarded as smectic G, E, H, and so on because the M1 phase is characterized as the smectic B phase. The M1−M2 transition begins as dirt on the surface of the morphology in the M1 phase. It is therefore possible that the M2 phase could be identified as the smectic G phase.

The difference between $m = 5$ and $m \ge 13$, which did not exhibit a mesophase−mesophase transition, was observed in the optical texture. The textures for F10H5 and F10H15 are shown in Figure 3. As shown in Figure 3a,b, the former was a mosaic pattern and the latter a sand texture. This difference indicates a change in the molecular orientational structure.

**Change in Entropy.** Figure 4 shows a change in the entropy at the clearing temperature ($\Delta S_I$) and at the transition temperature from the M2 to M1 phase ($\Delta S_{M2-M1}$) with increases in the chain length for F10H*m*, in addition to the results of F12H*m*.[6] A remarkable difference in the entropy was found between these materials, even though these compounds have the same constitution, except for two carbons linked to the fluorine atoms.

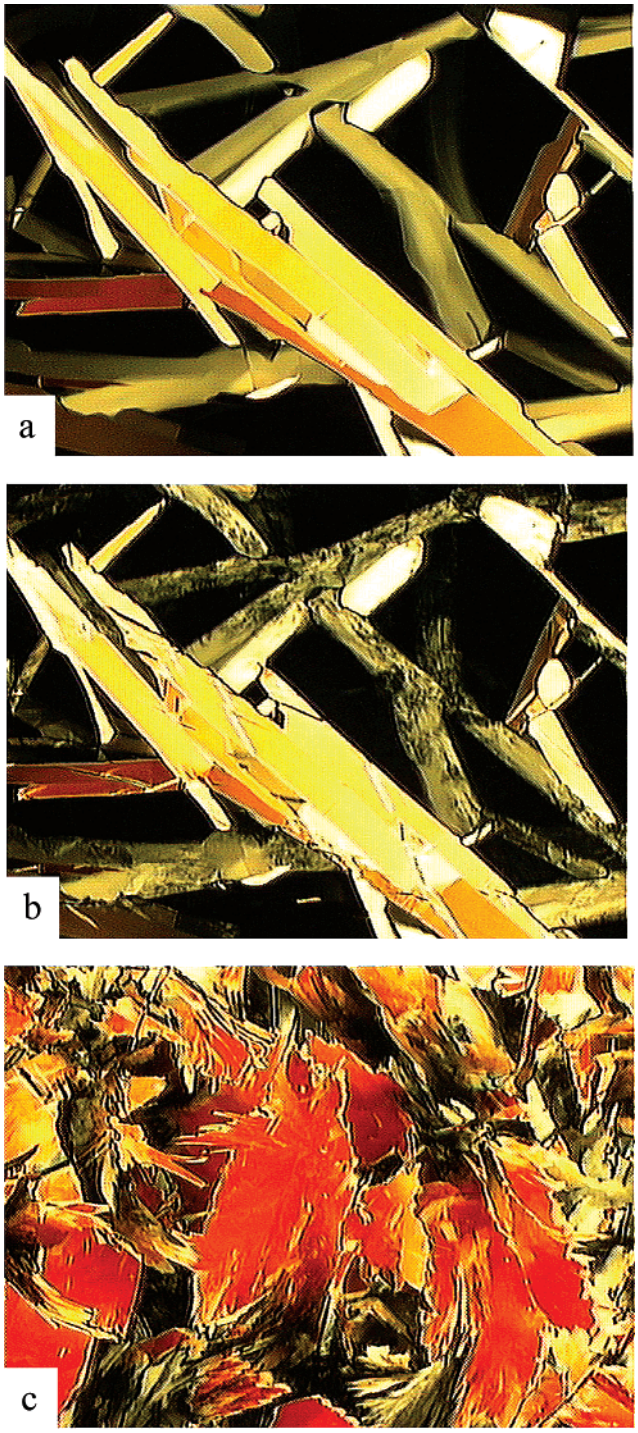


**Figure 2.** Optical textures for F10H10 observed between the crossed polars: (a) specimen at 330.5 K corresponding to the M1 phase during the first cooling; (b) specimen at 297.0 K corresponding to the M2 phase after further cooling; (c) the same area of viewing after one more day at 297.1 K.

With respect to F10H*m*, $\Delta S_I$ strongly increased with the number of methylene units in the hydrocarbon segment, while $\Delta S_{M2-M1}$ tended to increase with the number of methylene units. However, the change in $\Delta S_{M2-M1}$ was smaller than that for the clearing point. The value of the slope in $\Delta S_I$ for F10H*m* was significantly close to that for the *n*-alkanes. On the other hand, F12H*m* showed that $\Delta S_I$ was almost constant for each hydrocarbon number. Höpken et al.[6] have concluded that the transition for the clearing is primarily due to the disordering of the fluorocarbon segment, while the chain length dependence of $\Delta S_{M2-M1}$ indicates a disordering of the hydrogen segment. Both $F(CF_2)_{10}F$

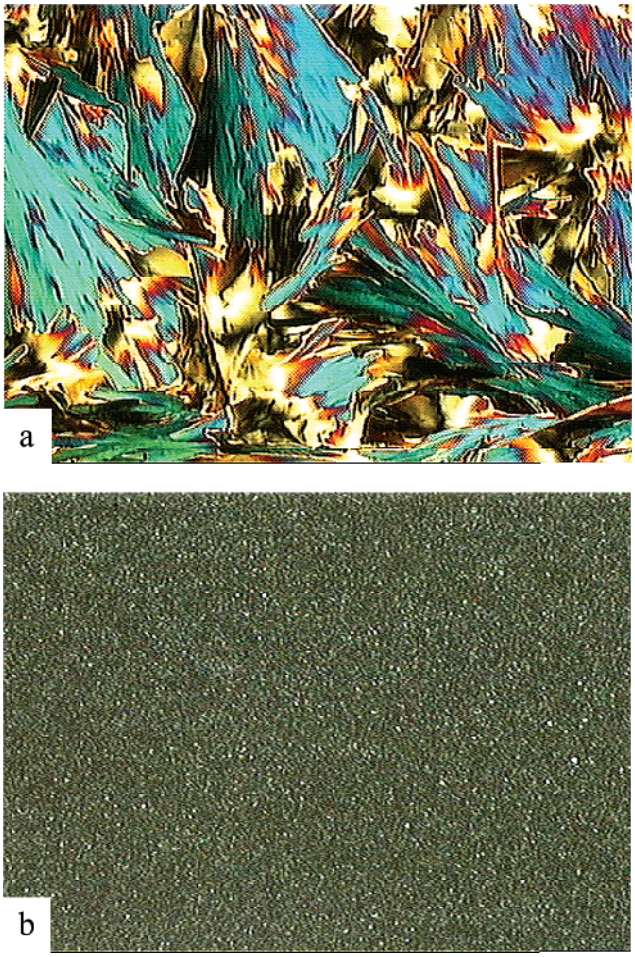


**Figure 3.** Optical textures for F10H5 (a) and F10H15 (b) at room temperature as observed between the crossed polars.

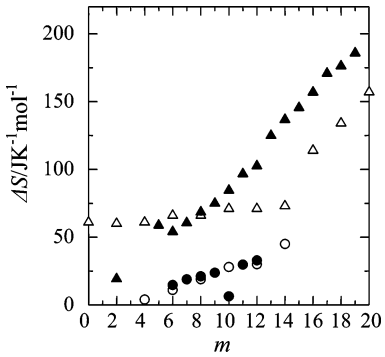


**Figure 4.** Change in the entropy at the clearing point (triangle symbols) and at the transition temperature from M2 to M1 phase (circle symbols) as a function of the length of *m* for F10H*m* (filled symbols) and F12H*m* (open symbols).

and $H(CH_2)_mH$ with $m = 6-12$ are liquid in the temperature range for the M1 phase. Furthermore, F10H*m* showed an approximately linear relationship between $\Delta S$ and the methylene units. Therefore, the $\Delta S_I$ for F10H*m* would be dominated by the disorder of the entire molecule, not just by the fluorinated segments. The M2−M1 transition would be primarily caused by the change in the molecular packing due to the change in the thermally induced mobility of both segments, as will be discussed below. In addition, the dielectric measurement also indicate a significant difference in molecular mobility between F10H10 and F12H8.[15] Therefore, the difference in these results between F10H*m* and F12H*m* leads us to conclude that there is a difference in the transition process.

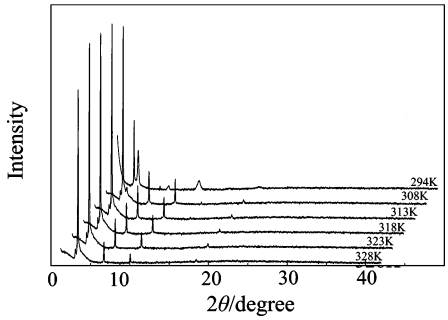


**Figure 5.** X-ray diffraction pattern for F10H9 at various temperatures.

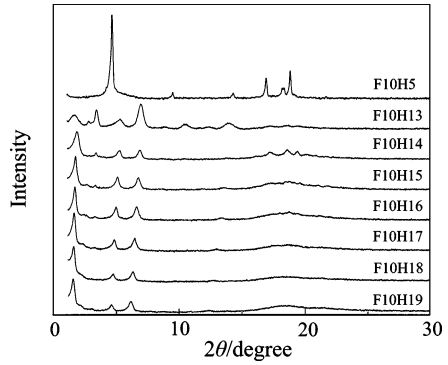


**Figure 6.** X-ray diffraction pattern for F10H*m* at room temperature.

In addition, the value of $\Delta S_{M2-M1}$ for F10H10 was clearly out of line with the other points and was extremely small. This difference was caused by the kinetic barrier associated with the molecular rearrangement. This value became the expected ordinary value due to the long period between the first cooling and second heating in the DSC measurement at the transition point.

**X-ray Diffraction.** Figure 5 shows the X-ray diffraction patterns at various temperatures for F10H9. The sharp X-ray scattering consisting of the first to third order in the M1 phase indicates that the molecules are arranged in a well-developed layer structure. A reflection in the high-angle region, $2\theta = 18.51°$, can be assigned to represent the intermolecular spacing. With increasing temperature, the distance between the adjacent molecules increased. The value of the intermolecular spacing was ~5.53 Å and approximately equal to 5.66 Å in the hexagonal structure of poly(tetrafluoroethylene) above room temperature.[20] This result shows that the lateral distance corresponds to a distance between the fluorinated segments for the semifluorinated *n*-alkanes. Adjacent molecules should be arranged such that fluorine−hydrogen contacts are minimized due to the mutual incompatibility of each segment. Therefore, the arrangement of the molecules in the M1 phase would be similar to parallel packing, where the fluorinated segments are aligned next to one another. Two first-order reflections at small angles were observed at room temperature corresponding to the M2 phase. Similar X-ray diffraction patterns were also obtained in the M1 phases of F10H*m*, except for F10H9. In contrast, the small-angle region for $m = 5$ consisted of a sharp reflection characterizing the single-crystal packing. These results lead us to conclude that two different structures coexist at temperature below the M1−M2 transition temperature for $6 \leq m \leq 12$. The diffraction diagrams of the F10H*m* compounds, which have no mesophase−mesophase transition at room temperature, are shown in Figure 6. F10H*m* with $m \geq 14$ have an obvious and different X-ray diffraction pattern in the wide-angle region as well as in the small-angle diffraction when compared to F10H5 with the crystal X-ray diffraction pattern. The wide-angle X-ray diffraction pattern of F10H*m* with $m \geq 14$ showed the formation of a disordered molecular orientation. The long alkyl sequence led to an increase in the disorder of the molecular orientation in the layers. These results are consistent with the optical micrographs data. The layer spacings $d_{M1}$ in the M1 phase and the molecular length $L_{cal}$ calculated from the ab initio calculation are given in Table 2. As to the conformation, the molecule consists of a planar zigzag hydrocarbon segment joined to a helical fluorinated carbon segment. The molecular lengths of F10H*m* for $m = 6-12$ were in agreement with the layer spacings, where the molecular length was considered as the distance between the centers of the terminal fluorine and the hydrogen atoms and their van der Waals radii.[21] From the optical texture and the observed hexagonal fashion, the M1 phase is identified as a smectic B where molecules undergo a fast rotational motion about their long axes. Figure 7 shows the most stable structure for F10H9, which was calculated by the ab initio calculation. The torsion angles were 17.0° and 0.59° for $\varphi$(C1C2C3C4) and $\varphi$(C9C10CH$_2$CH$_2$) of the terminal and central portions, respectively. Here the carbon atoms of the fluorinated sequence were numbered from the terminal atom. The other torsion angles of the helical fluorinated carbon segment were 17.9 ± 0.3°, which is almost comparable with the 18.1° for the perfluorohexane.[22]

Figure 8 shows the methylene unit dependence of the layer spacing for F10H*m*. Some distinct packing was observed depending on the number of *m*. As mentioned above, two different layer spacings coexisted in the M2 phase for $6 \leq m \leq 13$. The spacings for $5 \leq m \leq 11$ were shorter than the fully

**Table 2. Layer Spacing in the M1 Phase and the Calculated Molecular Length of F10H*m***

| *m* | $d_{M1}$/nm | $L_{cal}$/nm | $\Delta d$/nm[a] |
|---|---|---|---|
| 6 | 2.248 | 2.113 | 0.135 |
| 7 | 2.381 | 2.242 | 0.139 |
| 8 | 2.508 | 2.391 | 0.117 |
| 9 | 2.634 | 2.520 | 0.114 |
| 10 | 2.752 | 2.647 | 0.105 |
| 11 | 2.870 | 2.770 | 0.100 |
| 12 | 2.958 | 2.903 | 0.055 |

[a] $\Delta d = d_{M1} - L_{cal}$.

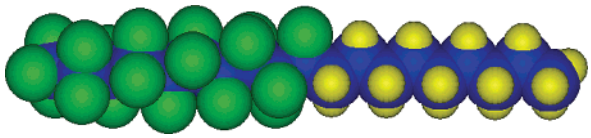

**Figure 7.** Optimized structure for F10H9. The structure was obtained by ab initio calculation with B3LYP/6-311G**.

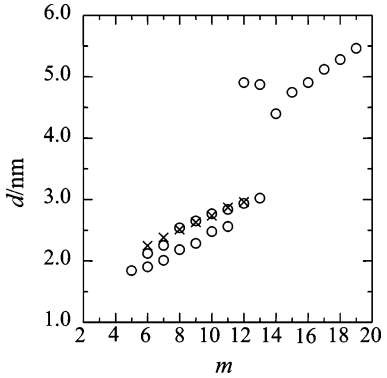


**Figure 8.** Layer spacings as a function of the length *m* of the hydrocarbon segment. The open circles represent the spacings at a temperature below a transition from the M2 to M1 phase whereas the cross symbols indicate those of the M1 phase.

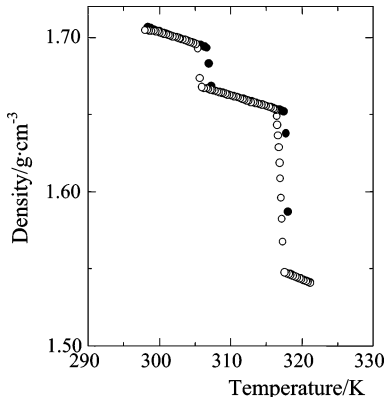


**Figure 9.** Density as a function of temperature for F10H6. The open and filled circles refer to the cooling and heating data, respectively.

extended molecular lengths. Therefore, it is very likely that the M2 phase consists of monolayers of tilted molecules. Furthermore, it is very interesting that the layer spacing, which was equal to that in the M1 phase, was observed at temperature in the M2 phase for $8 \leq m \leq 12$. This spacing as the molecular length suggests that the molecules transform in accordance with the tilt characteristics of the M2 phase but still remain stacked relative to the longitudinal displacement of the M1 phase by the sluggish kinetics of the transition. As discussed by Marczuk et al.,[8,9] the presence of two kinds of layer structures and the absence of Miller reflections in the diffraction data may lead us to conclude that the M2 phase adopts a ripple lamellar structure. The layer spacings for F10H12 and F10H13, except for one equal to that in the M1 phase, were longer than the molecular length and slightly less than 3 times the length of the longer segment of the molecule. Consequently, a tilted bilayer structure is formed in this phase.

**Density.** Figure 9 shows the temperature dependence of the density for F10H6 upon cooling and heating. The density variation process upon cooling was completely equal to that upon heating for all the studied compounds. These results indicate that F10H*m* is enantiotropic. The density change with temperature was found to be approximately linear. The rapid volume increases at the transition temperatures for the isotropic−M1 and M1−M2 transitions, significantly indicating a first-order phase transition. The density jump at the isotropic−M1 transition was greater than that for the M1−M2 transition. Therefore, the molecular packing for the M1 phase is considerably close to that for the M2 phase.

The temperature dependence of the density and the thermal expansion coefficient for F10H11 upon heating are shown in Figure 10. The transition temperature, which was determined from the maximum point of the thermal expansion coefficient, was consistent with the result from the DSC data. Only for F10H11 did we observe another very weak transition other than the M2−M1 and the M1−isotropic transition at temperature below the M2−M1 transition upon heating. This weak first-order phase transition may have been associated with a change in the unit-cell structure and was unambiguously determined by a dilatometry using a slower scanning speed than for the other measurements.

Figures 11 and 12 show the density and the molar volume as a function of the reduced temperature $T^*$ ($\equiv T/T_{I-M1}$) for the F10H*m* series on cooling, respectively. The absolute densities tend to decrease, and the molar volumes to increase, with chain length. The calculated molar volume per $CH_2$ unit gives values of 19.38 and 17.04 cm$^3$ mol$^{-1}$ for the isotropic and M1 phase, respectively. These values are comparable to the $\Delta V_{CH_2}$ value

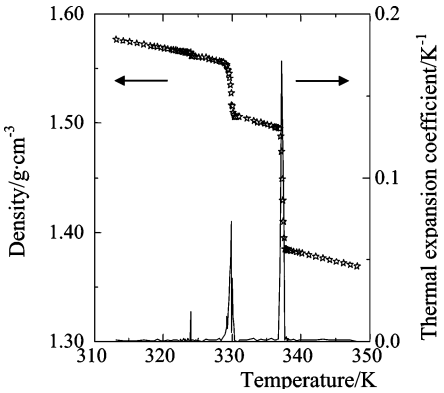


**Figure 10.** Density (star symbols) and the thermal expansion coefficient (solid line) as a function of the temperature for F10H11 upon heating.

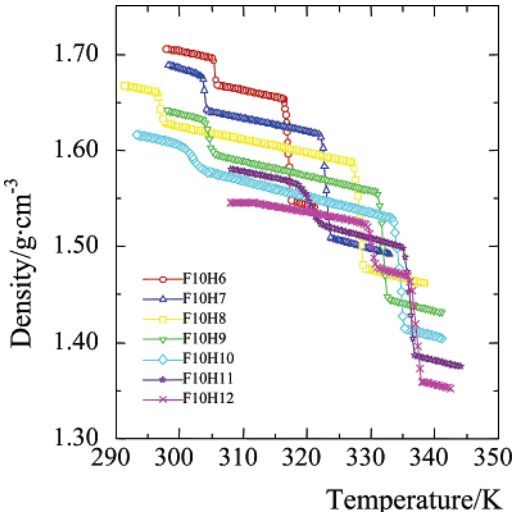


**Figure 11.** Densities as a function of temperature for the F10H*m* series upon cooling.

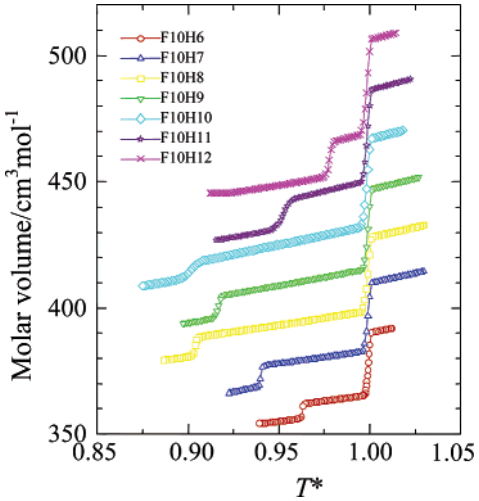


**Figure 12.** Molar volume as a function of the reduced temperature $T^*$ for the F10H*m* series upon cooling.

of 17.10 cm$^3$ mol$^{-1}$ for both the isotopic and smectic B phases for 4-bromo-*N*-(4-*n*-alkyloxybenzylidene)anilines.[23] The difference in the isotropic phase can be attributed to the fact that the semifluorinated *n*-alkane without a rigid needlike aromatic core in like the usual smetogenic molecules. However, it is very interesting that the molar volume increments per methylene unit in the M1 phase agree with that in the smectic B phase.

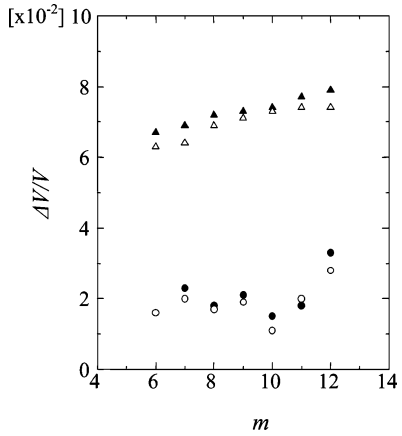


**Figure 13.** Volume changes at the M2−M1 transition (circles) and the M1−I transition (triangles) vs the number of carbon atoms in the alkyl chain for F10H*m*. The open and filled symbols refer to the data upon cooling and heating, respectively.

As reported by Viney et al.,[4] the correspondence of the exotherm to the M1−M2 transition upon cooling was not observed in the DSC. However, the density measurement was able to reveal the density jump at the M1−M2 transition. In fact, the slope of the density change at the M1−M2 transition for F10H10 was gentler than that for the other compounds. Therefore, the transition between the ordered phases upon cooling must release the latent heat over a wide range of temperature and time; no such transition would be detected in the DSC.

To determine the molecular packing in each phase, it is necessary to estimate the volume jump at the transition temperature. The actual volume jump at a transition temperature is not easy to determine. This difficulty makes it necessary to employing the Klement−Cohen's equation to estimate the temperature dependence of the volume.[24] The volume was fitted by the following equation:

$$V = V_{\text{phase}} + A(T_t - T) + B|T_t - T|^{1/2}$$

where $V_{\text{phase}}$ is the volume at the transition point, $T_t$ is the transition temperature, and $A$ and $B$ are constants. The results for each phase transition are shown in Figure 13. The value upon cooling was almost the same as that upon heating. The even−odd variation in the volume jump was observed at only $T_{M1-M2(M2-M1)}$. The compounds with odd-numbered carbons in the alkyl chain exhibit a larger volume jump than those with the even-numbered carbons. The even−odd phenomenon is attributable to the difference in the tilted angle in the M2 phase. The volume jump is generally associated with the transition enthalpy and entropy. Figure 4 indicates a satisfactory correspondence between the transition entropy and volume jump both at $T_{M2-M1}$ and $T_{M1-I}$, excluding the even−odd variation. The volume jump at $T_{I-M1(M1-I)}$ monotonically increased with the chain length. Those at the M2−M1 transition were approximately constant except for $m = 12$, which was fairly large. Needless to say, the result for F10H12 was associated with the formation of a bilayer structure in the M2 phase. Therefore, as mentioned above, we suggest that the M2−M1 transition is primarily due to a change in the molecular packing due to structural rearrangement, while the chain length dependence of the volume jump for the clearing indicates a disordering of the entire molecule, not each segment.

The volume jump indicates that the same molecular packing occurred for all materials in the M1 phase. The magnitude ($\Delta V = 31.0$ cm$^3$ mol$^{-1}$) was considerably higher than that ($\Delta V = 14.8$ cm$^3$ mol$^{-1}$) of conventional liquid crystalline compounds with the core rings like 4-iode-*N*-(4-*n*-alkyloxybenzylidene)-anilines.[23]

## Conclusions

A homologous series of semifluorinated *n*-alkanes, $F(CF_2)_{10}(CH_2)_mH$, with $2 \le m \le 19$, were synthesized and characterized repeating the phase transition behavior using a polarizing microscope, DSC, X-ray diffraction, and dilatometry. Ab initio calculation was used to evaluate the stable structure in order to determine the layer spacing and conformation. A thermal analysis showed the presence of a smectic−smectic phase transition, with the number of methylene units ranging from 6 to 12. The temperatures for the mesophase−mesophase transition varied depending on the length of the hydrocarbon segments.

The M1 phase was identified as the smectic B phase on the basis of the layer spacing being close to a sharp wide-angle reflection in the X-ray diffraction, and a texture characteristic of smectic B was revealed by microscopic observation. The calculated molecular length also supports this result. The M2 phase consisted of partially and fully transformed phases and was found to be a tilted smectic phase like G, where the molecular axes were tilted with respect to the layer normal or rippled. $F(CF_2)_{10}(CH_2)_mH$ where $6 \le m \le 12$ melted in a two-step process. In the first step, the molecular packing change brings about a change in the thermally induced mobility for both segments. The second step corresponds to the disordering for the entire molecule. The extremely slow kinetic process at the M1−M2 transition was observed for only F10H10. The density change clearly indicated that the transition rate was much slower than those for the other semifluorinated *n*-alkanes. The kinetic process was also observed in the optical and thermal analyses. The absolute densities tended to decrease, and the molar volumes increased with the chain length. The molar volume incremented by one methylene unit in the M1 phase agreed with that in the smectic B phase for conventional liquid crystalline compounds. The volume jump showed that all compounds had the same packing in the M1 phase. The difference in the entropy and density results between F10H*m* and F12H*m* suggests a difference in the transition process.

**Acknowledgment.** Gratitude is expressed to Mr. Y. Yamada and Mr. H. Yamaguchi for the dilatometry measurements.

## References and Notes

(1) Rabolt, J. F.; Russell, T. P.; Twieg, R. J. *Macromolecules* **1984**, *17*, 2786.
(2) Russell, T. P.; Rabolt, J. F.; Twieg, R. J.; Siemens, R. L.; Farmer, B. L. *Macromolecules* **1986**, *19*, 1135.
(3) Mahler, W.; Guillon, D.; Skoulios, A. *Mol. Cryst. Liq. Cryst. Lett.* **1985**, *2*, 111.
(4) Viney, C.; Russell, T. P.; Depero, L. E.; Twieg, R. J. *Mol. Cryst. Liq. Cryst.* **1989**, *168*, 63.
(5) Viney, C.; Twieg, R. J.; Russell, T. P.; Depero, L. E. *Liq. Cryst.* **1989**, *5*, 1783.
(6) Höpken, J.; Pugh, C.; Richtering, W.; Möller, M. *Makromol. Chem.* **1988**, *189*, 911.
(7) Höpken, J.; Möller, M. *Macromolecules* **1992**, *25*, 2482.
(8) Marczuk, P.; Lang, P. *Macromolecules* **1998**, *31*, 9013.
(9) Marczuk, P.; Lang, P.; Möller, M. *Colloids Surf., A* **2000**, *163*, 103.
(10) Geppi, M.; Pizzanelli, S.; Veracini, C. A.; Cardelli, C.; Tombari, E.; Nostro, P. L. *J. Phys. Chem. B* **2002**, *106*, 1598.
(11) Gaines, G. L., Jr. *Langmuir* **1991**, *7*, 3054.
(12) El Abed, A.; Pouzet, E.; Fauré, M.-C.; Sanière, M.; Abillon, O. *Phys. Rev. E* **2000**, *62*, 5895.
(13) Ulman, A. *Chem. Rev.* **1996**, *96*, 1553.

(14) Tamada, K.; Ishida, T.; Knoll, W.; Fukushima, H.; Colorado, R., Jr.; Graupe, M.; Shmakova, O. E.; Lee, T. R. *Langmuir* **2001**, *17*, 1913.
(15) Wong, D.; Lois, N. *Semin. Ophthalmol.* **2000**, *15*, 25.
(16) Araki, K.; Satoh, K.; Kondo, S. *Mol. Cryst. Liq. Cryst.* **1996**, *281*, 123.
(17) Araki, K.; Satoh, K.; Kondo, S. *Mol. Cryst. Liq. Cryst.* **1997**, *302*, 369.
(18) Guillon, D.; Skoulios, A. *Mol. Cryst. Liq. Cryst.* **1977**, *39*, 139.
(19) Gaussian 03, Revision B.03: Frisch, J.; Trucks, G. W.; Schlegel, H. B.; Scuseria, G. E.; Robb, M. A.; Cheeseman, J. R.; Montgomery, J. A., Jr.; Vreven, T.; Kudin, K. N.; Burant, J. C.; Millam, J. M.; Iyengar, S. S.; Tomasi, J.; Barone, V.; Mennucci, B.; Cossi, M.; Scalmani, G.; Rega, N.; Petersson, G. A.; Nakatsuji, H.; Hada, M.; Ehara, M.; Toyota, K.; Fukuda, R.; Hasegawa, J.; Ishida, M.; Nakajima, T.; Honda, Y.; Kitao, O.; Nakai, H.; Klene, M.; Li, X.; Knox, J. E.; Hratchian, H. P.; Cross, J. B.; Adamo, C.; Jaramillo, J.; Gomperts, R.; Stratmann, R. E.; Yazyev, O.; Austin, A. J.; Cammi, R.; Pomelli, C.; Ochterski, J. W.; Ayala, P. Y.; Morokuma, K.; Voth, G. A.; Salvador, P.; Dannenberg, J. J.; Zakrzewski, V. G.; Dapprich, S.; Daniels, A. D.; Strain, M. C.; Farkas, O.; Malick, D. K.; Rabuck, A. D.; Raghavachari, K.; Foresman, J. B.; Ortiz, J. V.; Cui, Q.; Baboul, A. G.; Clifford, S.; Cioslowski, J.; Stefanov, B. B.; Liu, G.; Liashenko, A.; Piskorz, P.; Komaromi, I.; Martin, R. L.; Fox, D. J.; Keith, T.; Al-Laham, M. A.; Peng, C. Y.; Nanayakkara, A.; Challacombe, M.; Gill, P. M. W.; Johnson, B.; Chen, W.; Wong, M. W.; Gonzalez, C.; Pople, J. A. Gaussian, Inc., Pittsburgh, PA, 2003.
(20) Sperling, L. H. *Introduction to Physical Polymer Science*; John Wiley & Sons: New York, 1986; p 159.
(21) Bondi, A. *J. Phys. Chem.* **1964**, *68*, 441.
(22) Smith, G. D.; Jaffe, R. L.; Yoon, D. Y. *Macromolecules* **1994**, *27*, 3166.
(23) Seurin, P.; Guillon, D.; Skoulios, A. *Mol. Cryst. Liq. Cryst.* **1981**, *65*, 85.
(24) Klement, W., Jr.; Cohen, L. H. *Mol. Cryst. Liq. Cryst.* **1974**, *27*, 359.

MA052411B